Novel Composites of α-Fe_2O_3 Tetrakaidecahedron and Graphene Oxide as an Effective Photoelectrode with Enhanced Photocurrent Performances

*Shaoxiong Liu, Lingxia Zheng, Pingping Yu, Sancan Han, and Xiaosheng Fang**

Novel composites composed of α-Fe_2O_3 tetrakaidecahedrons and graphene oxide have been easily fabricated and demonstrated to be efficient photoelectrodes for photoelectrochemical water splitting reaction with superior photocurrent response. α-Fe_2O_3 tetrakaidecahedrons are facilely synthesized in a green manner without any organic additives and then modified with graphene oxide. The morphological and structural properties of α-Fe_2O_3/graphene composite are intensively investigated by several means, such as X-ray diffraction, field-emission scanning electron microscope, transmission electron microscope, X-ray photoelectron spectroscopy, Fourier Transform infrared spectroscopy, and Raman spectroscopy. The tetrakaidecahedronal hematite particles have been indicated to be successfully coupled with graphene oxide. Systematical photoelectrochemical and impedance spectroscopy measurements have been carried out to investigate the favorable performance of α-Fe_2O_3/graphene composites, which are found to be effective photoanodes with rapid, steady, and reproducible feature. The coupling of graphene with α-Fe_2O_3 particles has greatly enhanced the photoelectrochemical performance, resulting in higher photocurrent and lower onset potential than that of pure α-Fe_2O_3. This investigation has provided a feasible method to synthesize α-Fe_2O_3 tetrakaidecahedron and fabricate an efficient α-Fe_2O_3/graphene photoelectrode for photoelectrochemical water oxidation, suggesting a promising route to design noble metal free semiconductor/graphene photocatalysts.

1. Introduction

The photoelectrochemical (PEC) water splitting reaction has been regarded as one of the most promising strategies to convert solar energy into chemical energy, which offers the hope of resolving the potential energy crisis by convenient hydrogen production from natural water and sunlight.[1,2] The PEC water splitting reaction generally carries out through a semiconductor-based photoanode which absorbs incident light photons and produce photogenerated electron–hole pairs. Hematite (α-Fe_2O_3) is considered as a very interesting semiconductor material for PEC photoanode due to its promising properties of high stability in most aqueous solutions, broad visible-light absorption up to 590 nm, environmental friendliness, abundance in the earth, and low cost.[3–5] With a favorable bandgap (1.9–2.2 eV), the absorption efficiency of hematite to solar irradiation is up to 40%.[6,7] Furthermore, hematite has been predicted to theoretically achieve a high photocurrent of 12.6 mA cm^{-2} for water splitting and reach a solar-to-hydrogen efficiency up to 15.5% under AM 1.5G solar irradiation.[8] Although there are plenty of advantages of hematite acting as photoanodes, the practical application of hematite-based photoanodes for solar water splitting is limited by certain factors, such as poor absorption-coefficient, low electrical conductivity, short excited-state lifetime ($\approx 10^{-12}$ s), short hole diffusion length (2–4 nm), fast electron–hole pairs recombination rate, and poor oxygen evolution reaction kinetics.[9] Accordingly, it is necessary to exploit efficient and convenient approach to fabricate hematite-based photoanode for PEC water oxidation process.

Numerous nanostructures of α-Fe_2O_3 with different morphologies, such as nanoparticles,[10] nanorods,[11] nanowires,[12] nanoplates,[7] nanoflowers,[13] and nanocubes,[14] have been reported to be controllable synthesized and intensively investigated in the field of lithium ion batteries,[15,16] p-type and n-type field effect transistors,[17] H_2S chemical sensors,[18] red pigment for porcelain,[19] photodegradation,[7] and PEC water splitting.[20–22] Nevertheless, the precise synthesis of α-Fe_2O_3 polyhedrons only has been reported a few times owing to their intricate crystal structure.[23,24] The synthesis of tetrakaidecahedronal and oblique parallelepiped iron oxide crystal by a hydrothermal process of potassium ferricyanide and viscous macromolecules has been demonstrated.[25] The dodecahedral and octodecahedral α-Fe_2O_3 particles by a hydrothermal reaction of ferric chloride and F^- anions were successfully prepared.[26] The other means and other morphology, such as truncated hexagonal bipyramid, hexagonal bipyramid, and quasi-cubic particles, also have been reported.[27–29] The gas sensor based on α-Fe_2O_3 oblique parallelepipeds nanoparticles was fabricated, which showed higher sensitivity, shorter recovery time,

Dr. S. X. Liu, Dr. L. X. Zheng, Dr. P. P. Yu, Dr. S. C. Han, Prof. X. S. Fang
Department of Materials Science
Fudan University
Shanghai 200433, P. R. China
E-mail: xshfang@fudan.edu.cn

DOI: 10.1002/adfm.201505554

and better reproducibility for ethanol and acetone detection than commercial α-Fe_2O_3 powders.[30] The superiority has been ascribed to the special surface structure of polyhedral nanocrystals. The application of α-Fe_2O_3 polyhedron to photoelectrochemical field has been extended.[31] They have fabricated the photoanode based on dodecahedral α-Fe_2O_3 nanocrystals which showed high photoelectrocatalytic activity and fine stability under visible light irradiation. The further investigation of α-Fe_2O_3 polyhedron in PEC process is highly promising and necessary. Other than nanostructures mentioned above, massive investigations have been devoted to improve the activity of α-Fe_2O_3-based materials, such as metal hybrid,[32] heterojunction assembling,[20] and surface modification with Co-Pi or IrO_2.[33,34] Meanwhile, coupling with graphene has been regarded as a feasible route for efficient activity improvement of α-Fe_2O_3-based materials. Graphene can serve as an important charge transfer medium, which slows the recombination rate of electron–hole pairs and accelerate charge transfer rate of electrons and surface adsorbed amount of chemical molecules through π–π interaction.[35,36] A α-Fe_2O_3 nanorods/graphene/$BiV_{1-x}Mo_xO_4$ core/shell heterojunction array as an efficient visible light-driven photoanode for photoelectrochemical water splitting has been reported.[37] Hexagonal α-Fe_2O_3/graphene composites have been synthesized through one-step hydrothermal reaction, which exhibited enhanced photocatalytic activity for pollutant degradation.[7] A net-like hematite nanoparticles/graphene oxide (GO) composite with much higher photocatalytic activity than pure α-Fe_2O_3 has been fabricated.[38] Accordingly, the fabrication of α-Fe_2O_3 polyhedron/graphene composites with enhanced PEC activity is desirable and practical applications.

Herein α-Fe_2O_3 tetrakaidecahedron/graphene oxide (α-Fe_2O_3/GO) composites are facilely fabricated in which α-Fe_2O_3 particles are supported on the graphene sheets. The α-Fe_2O_3 tetrakaidecahedrons prepared by a hydrothermal process without any organic additives display good crystallinity, which are modified by graphene oxide afterward. Other than the previous reports involving viscous macromolecules,[25,27,28] F^- anion,[26] and diethylenetriamine,[31] the hydrothermal synthesis of α-Fe_2O_3 tetrakaidecahedrons is specially facile and environmental, which only uses $FeCl_2{\bullet}4H_2O$, NaOH, and ultrapure H_2O as reaction precursors. Through photoelectrochemical investigation, this kind of α-Fe_2O_3/graphene photoelectrode shows superior photocurrent response than that of pure α-Fe_2O_3 with higher photocurrent and lower onset potential. The higher PEC performances of α-Fe_2O_3/graphene composites have been ascribed to the coupling of graphene, which facilitate the charge transfer and separation, and hinder the charge recombination of photogenerated electron–hole pairs.

2. Results and Discussion

As shown in **Figure 1**, the crystal phases of pure α-Fe_2O_3 polyhedrons and three kinds of α-Fe_2O_3/GO nanohybrids with different GO weigh ratios of 5%, 10%, and 15% (labeled as α-Fe_2O_3/GO 1, α-Fe_2O_3/GO 2, and α-Fe_2O_3/GO 3, respectively) were studied by X-ray diffraction (XRD). The diffraction peaks are all attributed to rhombohedral α-Fe_2O_3 phase, according

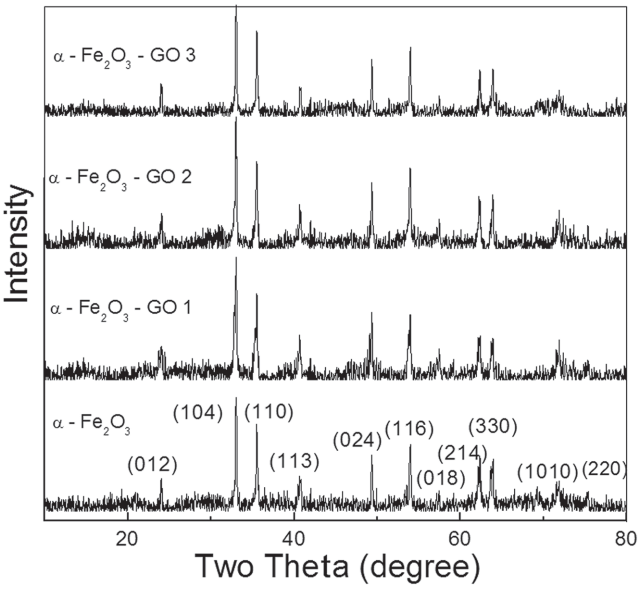

Figure 1. XRD patterns of the α-Fe_2O_3 and α-Fe_2O_3/graphene oxide (GO) 1, 2, 3 composites with different graphene oxide ratio of 5%, 10%, and 15%, respectively.

to the standard card JCPDS 33-0664. The peaks all display a strong and sharp feature, meaning that all nanocomposites are excellently crystallized. There are almost no apparent peak shift and other peak arising after α-Fe_2O_3 nanopolyhedrons coupling with graphene oxide, indicating that the complexation of α-Fe_2O_3 and graphene oxide has nearly no effects on the phase composition and crystallinity of α-Fe_2O_3 nanoparticles. The diffraction peaks at 24.0°, 33.0°, 35.5°, 40.7°, 49.3°, 54.0°, 57.6°, 62.3°, 63.9°, 71.8°, and 75.3° can be attributed to (012), (104), (110), (113), (024), (116), (018), (214), (300), (1010), and (220) crystal planes of α-Fe_2O_3 nanopolyhedrons, respectively.

The single-crystalline polyhedral α-Fe_2O_3 has been obtained by a simple hydrothermal procedure. **Figure 2**a–d shows the representative scanning electron microscopy (SEM) and transmission electron microscopy (TEM) images of pure α-Fe_2O_3 nanopolyhedrons and α-Fe_2O_3/GO 3 composite. The product in Figure 2a,b is SEM images showing their well-defined morphological features of tetrakaidecahedron with an average particle size of 700 nm broad and good size distribution. It can be seen that the obtained polyhedral nanocrystals are comprised of two hexagonal surfaces at the top and bottom and 12 slanted trapezoidal side-surfaces with 14 facets, 18 vertices, and 30 edges.[39,40] It is a highly symmetric tetrakaidecahedron of hexagonally bipyramidal shape. Figure 2c,d shows the TEM image of α-Fe_2O_3 nanopolyhedron and the corresponding selected area electron diffraction (SAED) pattern in the inset. The diffraction spots of SAED pattern can be ascribed to (110), (211), (214), and (104) planes and/or the equivalent planes. The sharp diffraction feature of inset indicates the single-crystalline structure of the polyhedral particle. In Figure 2d, two kinds of lattice spacing can be clearly identified with the interplane distances of 0.25 and 0.37 nm, corresponding to the interplane distances of (110) and (1–12) planes, which are consistent with the XRD and SAED results. In Figure 2e,f, the TEM images

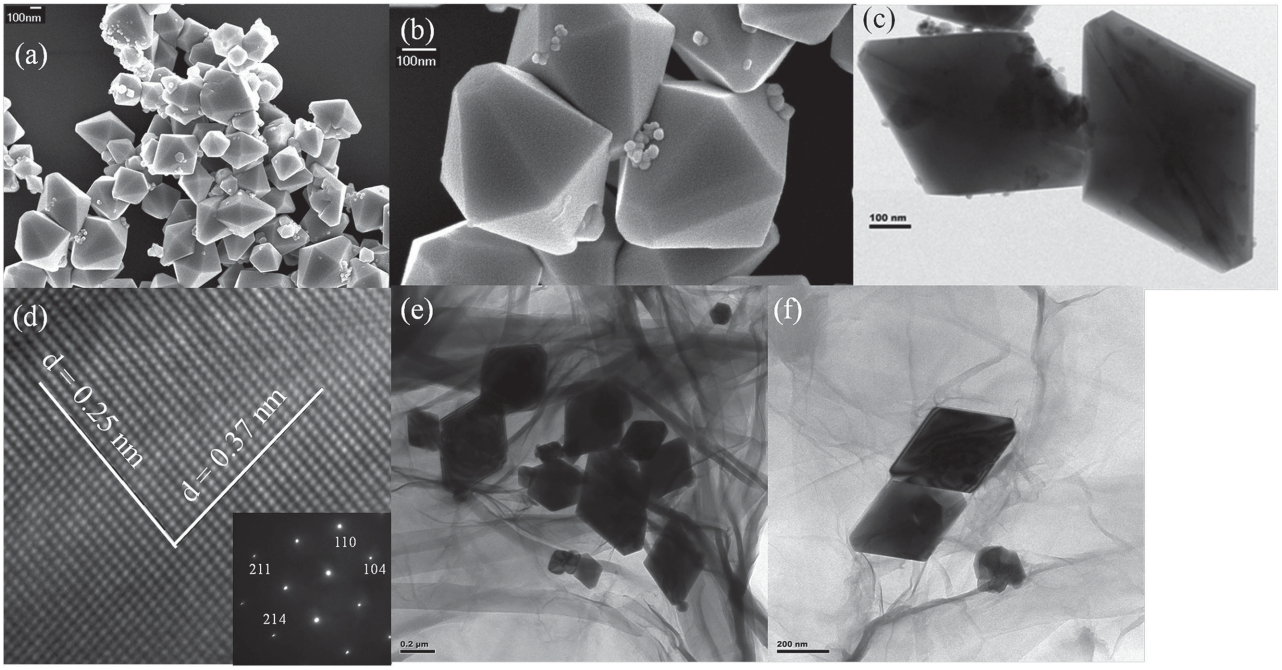

Figure 2. SEM and TEM images of the α-Fe_2O_3 and α-Fe_2O_3/graphene oxide (GO) composites with graphene oxide ratio of 15%. a,b) SEM images of pure α-Fe_2O_3. c,d) TEM images of pure α-Fe_2O_3. The inset in (d) is the corresponding SAED pattern. e,f) TEM images of α-Fe_2O_3/GO composite.

of α-Fe_2O_3/GO composite show that the α-Fe_2O_3 nanopolyhedrons are dispersed on the graphene oxide nanosheets. The graphene oxide nanosheets in α-Fe_2O_3/GO composite can serve as a stable supporting substrate to anchor α-Fe_2O_3 particles, implying there is a strong interaction between graphene oxide and α-Fe_2O_3 particles. Acting as the anchoring sites, the carboxyl and hydroxyl groups on the surface of graphene oxide can coordinate with α-Fe_2O_3 particles, leading to the immobilization of α-Fe_2O_3 particles on the whole graphene oxide nanosheets.[41]

The elemental components of the α-Fe_2O_3/GO composite are further characterized by X-ray photoelectron spectroscopy (XPS) measurements. **Figure 3**a displays a typical XPS profile of α-Fe_2O_3/GO 3 composite. The XPS figure feature demonstrates that the nanocomposite is absolutely composed of three elements of Fe, O, and C. No other elemental peak signals are detected by the XPS spectrum. The core level binding energy located at 713.1 and 726.8 eV is shown in the Fe 2p spectrum in Figure 3b, corresponding to Fe 2p1/2 and Fe 2p3/2 core level of the α-Fe_2O_3 nanopolyhedrons, respectively.[42] Meanwhile, the satellite peak centered at 719.0 eV should be solely attributed to the existence of Fe^{3+} ions in α-Fe_2O_3.[27,42] As shown in Figure 3c, the strong C 1s peak comes from the graphene in the composite. In the C 1s spectrum, the peaks at 284.6, 286.5, and 288.7 eV are attributed to C—C, C=O, and O—C=O configurations, respectively.[7]

Fourier transform infrared (FT-IR) spectroscopy is also employed to study the chemical structure comparison between pure α-Fe_2O_3 and α-Fe_2O_3/GO 3 composites. As shown in **Figure 4**, there are several obvious peaks raised after the introduction of graphene oxide to α-Fe_2O_3. The broad band arising around 3420 cm^{-1} is attributed to hydroxyl groups of graphene oxide, indicating the sufficiently composition of graphene oxide and α-Fe_2O_3.[43] The peaks located at 1205 and 1717 cm^{-1} are assigned to the C=O and C—O stretching vibration band of COOH groups, respectively.[44] The specific feature peak of

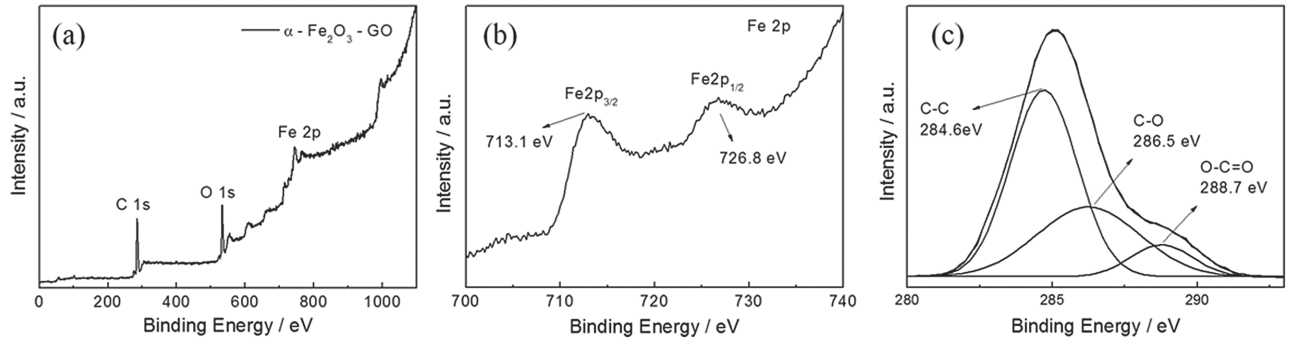

Figure 3. High-resolution XPS spectra of: a) general XPS, b) Fe 2p region, and c) C 1s region of α-Fe_2O_3/graphene oxide (GO) composite with graphene oxide ratio of 15%.

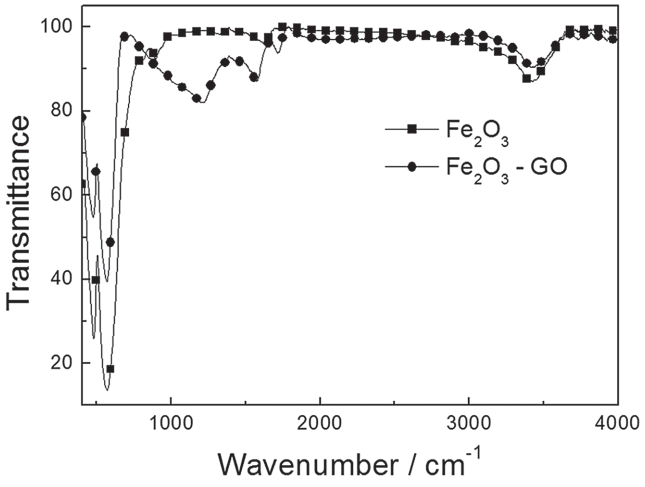

Figure 4. FT-IR transmittance spectra of the α-Fe_2O_3 and α-Fe_2O_3/graphene oxide (GO) composite with graphene oxide ratio of 15%.

aromatic C=C is detected at 1571 cm^{-1}.[45] These characteristic peaks of FTIR spectra demonstrate the well complexation of α-Fe_2O_3/GO composite.

The Raman spectra of α-Fe_2O_3 and α-Fe_2O_3/GO 3 composite are displayed in **Figure 5**. All characteristic bands of α-Fe_2O_3 in the range of lower wavenumber are detected in the Raman spectra of α-Fe_2O_3 and α-Fe_2O_3/GO composites. The bands located at 227 cm^{-1} are attributed to A_{1g} symmetry vibrations of α-Fe_2O_3, while the bands located at 296, 411, and 605 cm^{-1} are attributed to the E_g symmetry vibrations of α-Fe_2O_3.[7] In the α-Fe_2O_3/GO composite, two peaks located at 1320 cm^{-1} and 1624 cm^{-1} arising and the decrease of all the fundamental Raman bands of α-Fe_2O_3 indicate the sufficient combination of α-Fe_2O_3 nanopolyhedrons with the graphene layer. The specific bands at 1320 cm^{-1} and 1624 cm^{-1} are attributed to disorder band coupled with structural defects in graphene (D band) and ordered scattering of the E_{2g} phonon of sp^2C atoms of graphene (G band), respectively,[46] implying that the structure of graphene is maintained in α-Fe_2O_3/GO composite after the hydrothermal reaction. The higher intensity of D band than that of G band indicates the existence of high-density defects and structure disorder in graphene nanoplates.[7]

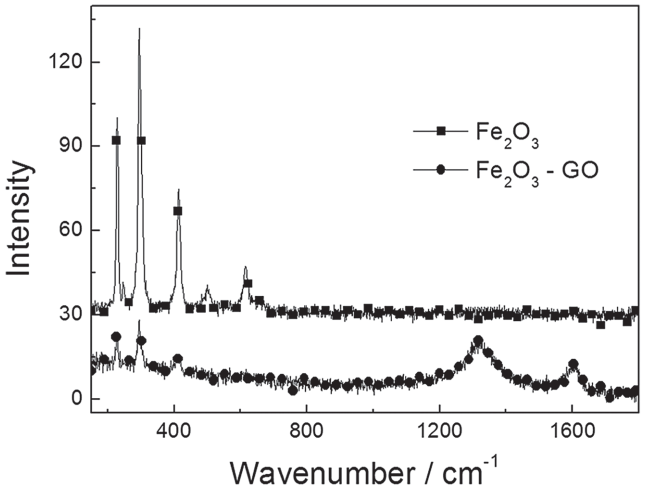

Figure 5. Raman spectra of the α-Fe_2O_3 and α-Fe_2O_3/graphene oxide (GO) composite with graphene oxide ratio of 15%.

With the steady polyhedral pure α-Fe_2O_3 and α-Fe_2O_3/graphene composites in hand, their PEC activity was further characterized with and without UV-light illumination. In the first place, the photoresponse performance of pure α-Fe_2O_3 is displayed in **Figure 6** by several means. The photocurrent density–potential curves (*I–V* curve) in Figure 6a obtained by linear sweep voltammetry indicate the strong enhancement of polarization current for the oxygen evolution reaction. The photocurrent of pure α-Fe_2O_3 electrode is about 3.8 times higher than that in dark with an obviously lower onset potential. Figure 6b displays the chopping photocurrent responses test of pure α-Fe_2O_3 electrode at const 1.7 V (vs reversible hydrogen electrode (RHE)), which shows a rapid, stable, and reproducible feature. Upon the UV-light illumination, a current spike rises immediately as the photoresponse for all the dark-light switches due to the fast impact of light excitation, and then the photocurrent quickly decays to a stable state less than 1 s. The dependence plot of photocurrent as a function of increasing potentials of pure α-Fe_2O_3 electrode under chopped light is displayed in Figure 6c. The rapid photocurrent response reappears just as that in Figure 6b at const potential, indicating the fine photoresponse and good applicability of pure α-Fe_2O_3 electrode in variational potential. The enhancement of photocurrent of pure α-Fe_2O_3 photoelectrode has been further investigated by EIS (electrochemical impedance spectroscopy) measurements in Figure 6d, in which the radius of every arc can be related to the charge-transfer process at the studying electrode/electrolyte interface with the smaller radius corresponding to the lower charge-transfer resistance and faster electron transfer kinetics of the redox reacting.[47–49] For the pure α-Fe_2O_3 photoelectrode, the arc radius under UV-light illumination is obviously smaller than that in dark, which indicates a smaller charge-transfer resistance of α-Fe_2O_3 photoelectrode under illumination and leads to a strong enhancement of photocurrent than that in dark. The series of PEC investigation demonstrates that the α-Fe_2O_3 photoelectrode possesses a favorable photoresponse for PEC activity with a fast, steady, and reproducible feature, which can be attributed to its specific morphological and structural characteristic. The unique polyhedral nanostructure possesses abundant exposed (110) facets, which have been reported to display better photocatalytic activity than (012), (001) facets and higher PEC activity than commercial α-Fe_2O_3 nanoparticles.[14,31,50] And the large number of uncoordinated surface atoms around α-Fe_2O_3 polyhedron can offer plenty of active sites for the photoinduced reaction.[31] Good crystallinity of α-Fe_2O_3 polyhedrons also benefits the fast transfer of photogenerated carriers.[31]

In order to improve the PEC activity of pure α-Fe_2O_3 nanomaterials, graphene oxide was introduced to fabricate a series of α-Fe_2O_3/graphene oxide (α-Fe_2O_3/GO 1, 2, 3) nanocomposites with different graphene oxide mass ratios of 5%, 10%, and 15%. The PEC performance of α-Fe_2O_3/graphene oxide nanocomposites is investigated by photocurrent response tests systematically in **Figure 7**. Figure 7a displays current density–potential curves of α-Fe_2O_3/GO 1, 2, and 3 in Na_2SO_4 aqueous solution in dark. After introduction of graphene oxide, the

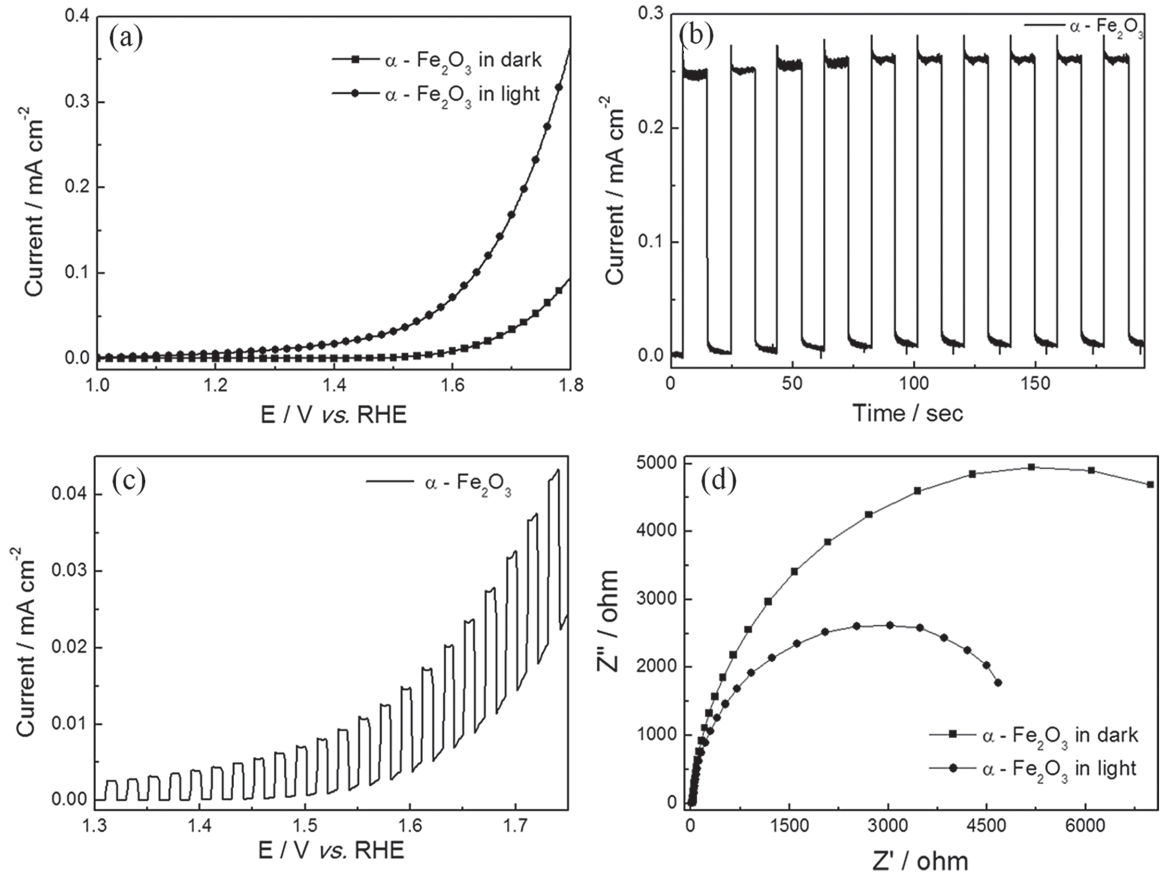

Figure 6. The photoelectrochemical performance of α-Fe_2O_3 electrode in Na_2SO_4 solution under Xe light after bubbling with high-purity N_2 for 30 min: a) linear sweep voltammetry curves of α-Fe_2O_3 electrode with and without UV–visible light illumination, scan rate: 10 mV s^{-1}. b) Photocurrent density–time curves of α-Fe_2O_3 electrode at the potential of 1.7 V (vs RHE) with UV–visible light illumination at an interval of 10 s on/off switch. (c) Linear sweep voltammetry curves of α-Fe_2O_3 electrode with UV–visible light illumination at an interval of 10 s on/off switch, scan rate: 1 mV s^{-1}. d) EIS Nyquist plots of α-Fe_2O_3 electrode with and without UV–visible light illumination.

three kinds of α-Fe_2O_3/graphene oxide electrodes all display higher current density than pure α-Fe_2O_3 electrode. Among all the graphene oxide modified α-Fe_2O_3 electrodes, the α-Fe_2O_3/GO 3 electrode reaches the highest current density of about 0.59 mA cm^{-2}, which is about 6.1 times of that of pure α-Fe_2O_3 electrode. The current density of the three kinds of α-Fe_2O_3/GO electrodes is approximate, indicating that the favorable effect of graphene oxide is really obvious. Other than the raised current density, the onset potentials of all α-Fe_2O_3/GO electrodes are close again and lower than that of pure α-Fe_2O_3 electrodes, which is in agreement with previous literatures.[51] The lower onset potentials of three α-Fe_2O_3/GO electrodes can be attributed to favorable effect of graphene oxide, which decrease the kinetic energy barrier of charge transfer among the interface of graphene oxide and α-Fe_2O_3.[34,52] The corresponding EIS measurements of the electrodes in Figure 7a are shown in Figure 7b. The three α-Fe_2O_3/GO electrodes show a smaller radius than that of pure α-Fe_2O_3 electrode, in which the radius of α-Fe_2O_3/GO 3 is smallest associating with its highest current density. This result demonstrates that the introduction of graphene decreases the charge-transfer resistance of composite materials, which agreed with the previous paper.[53,54] α-Fe_2O_3 with N-doped graphene has been coupled and found the charge transfer resistance decreased after the introduction of graphene.[54] This complex is responsible for the decrease of onset potential and increase of current density partly. The photocurrent response of α-Fe_2O_3/GO and pure α-Fe_2O_3 electrodes is displayed in Figure 7c, taking the α-Fe_2O_3/GO 3 electrode as representation. The photocurrent density of α-Fe_2O_3/GO 3 reaches 1.63 mA cm^{-2} at 1.8 V versus RHE, which is 4.39 times higher than that of pure α-Fe_2O_3 electrode in light and 2.67 times higher than current density in dark of itself. Upon UV-light illumination, the onset potential of α-Fe_2O_3/GO 3 also decreases slightly, which is consistent with that of pure α-Fe_2O_3 electrode in Figure 6a. The enhancement of photocurrent performance can be ascribed to the efficient electron collection and transformation feature of graphene oxide, which effectively impedes the recombination of photoinduced electron and hole.[55] The graphene can serve as an electron transfer channel, which offers a quick path to transfer more photogenerated electrons from α-Fe_2O_3 to charge collector.[56,57] The lower onset potential of α-Fe_2O_3/GO 3 electrode is associated with a smaller kinetic energy barrier for charge transfer at the electrode/electrolyte interface again, which can be attributed to the passivation effect of graphene oxide to α-Fe_2O_3. There is a passivation layer at the α-Fe_2O_3/GO interface, which facilitates the

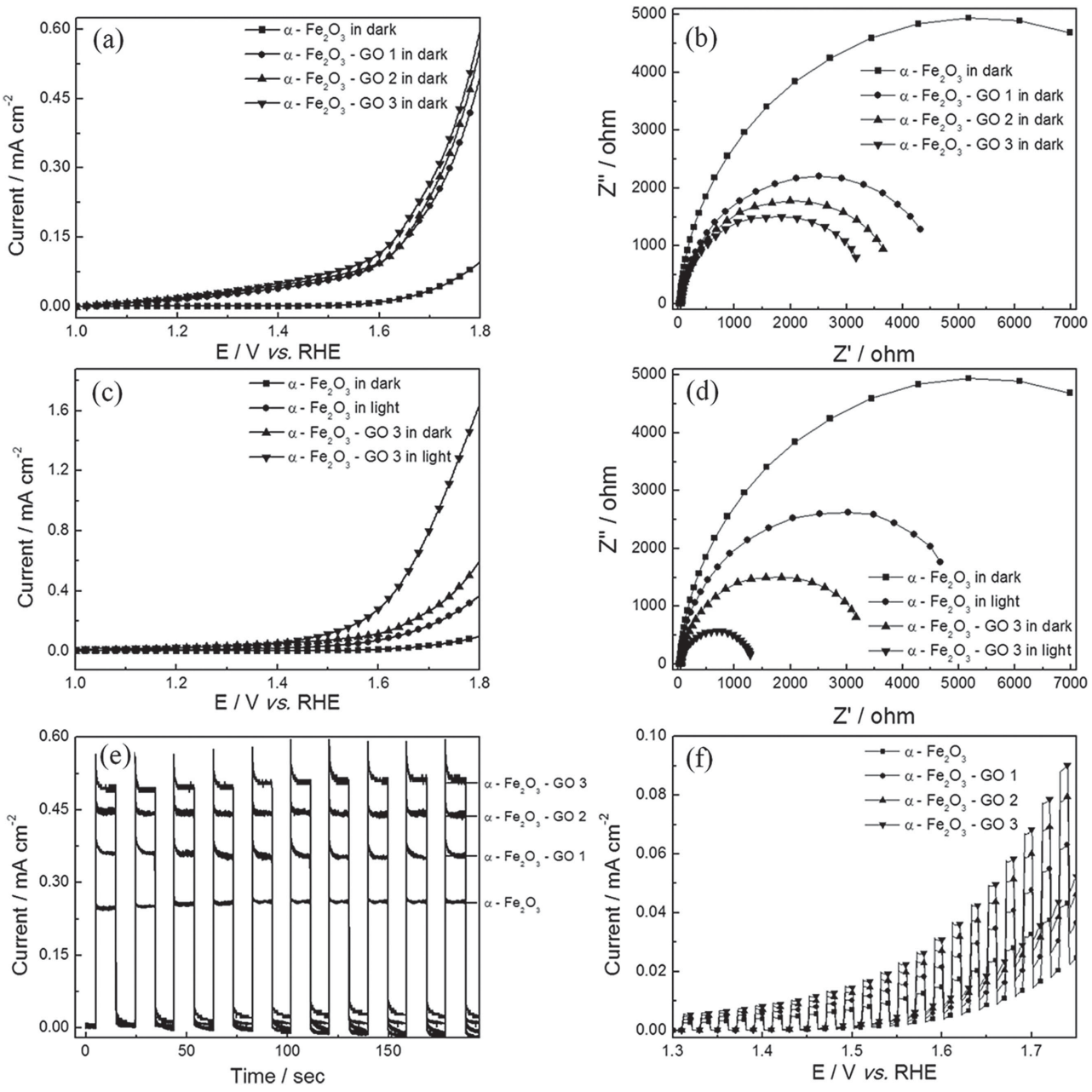

Figure 7. The photoelectrochemical performance of α-Fe_2O_3 and α-Fe_2O_3/GO electrodes in Na_2SO_4 solution under Xe light after bubbling with high-purity N_2 for 30 min (α-Fe_2O_3/GO 1, 2, 3 are denoted for α-Fe_2O_3/graphene oxide composites with different graphene oxide ratio of 5%, 10%, and 15%, respectively): a) linear sweep voltammetry curves of α-Fe_2O_3 and α-Fe_2O_3/GO 1, 2, 3 electrodes in dark, scan rate: 10 mV s^{-1}. b) EIS Nyquist plots of α-Fe_2O_3 and α-Fe_2O_3/GO 1, 2, 3 electrodes in dark. c) Linear sweep voltammetry curves of α-Fe_2O_3 and α-Fe_2O_3/GO 3 electrodes with and without UV–visible light illumination, scan rate: 10 mV s^{-1}. d) EIS Nyquist plots of α-Fe_2O_3 and α-Fe_2O_3/GO 3 electrodes with and without UV–visible light illumination. e) Photocurrent density–time curves of α-Fe_2O_3 and α-Fe_2O_3/GO 1, 2, 3 electrodes at the potential of 1.7 V (vs RHE) with UV–visible light illumination at an interval of 10 s on/off switch. f) Linear sweep voltammetry curves of α-Fe_2O_3 and α-Fe_2O_3/GO 1, 2, 3 electrodes with UV–visible light illumination at an interval of 10 s on/off switch, scan rate: 1 mV s^{-1}.

hole transfer through the interface.[55] Similar results have been demonstrated in silicon/graphene system, in which the single layer of graphene displayed protection and passivation effect.[58] The EIS Nyquist plots of α-Fe_2O_3/GO 3 and pure α-Fe_2O_3 electrodes are shown in Figure 7d. The smaller radius of the EIS curve of α-Fe_2O_3/GO 3 electrode in light than those of itself in dark and pure α-Fe_2O_3 electrode in light indicates the decrease in charge transfer resistance and improved transport behavior at the electrode/electrolyte interface.[59] The better transfer efficiency of photogenerated charge carrier can be associated with the higher photocurrent density of α-Fe_2O_3 with the help of graphene oxide. Owing to the superior electroconductivity, the

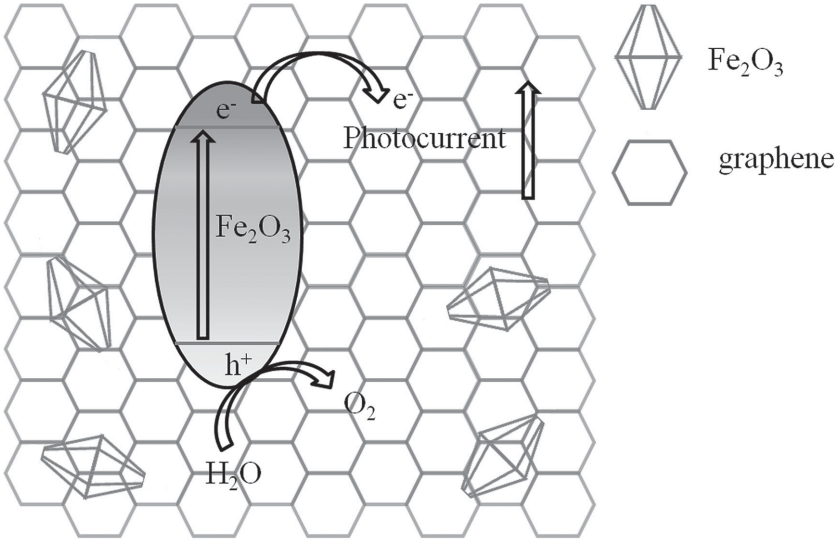

Figure 8. The mechanism illustration of photogenerated charge transfer and separation in the α-Fe_2O_3 tetrakaidecahedron/graphene oxide composite.

blending of graphene facilitates the charge transfer in the composite material and hinders the recombination of charge–hole pairs. Furthermore, the graphene sheets also benefit the collection and transportation of photogenerated holes, leading to the increase of photocurrent density.[60] These results clearly demonstrate the synergetic effect of graphene oxide and α-Fe_2O_3 nanopolyhedron to fabricate an efficient photoelectrode. The photocurrent density versus time curves of three α-Fe_2O_3/GO and α-Fe_2O_3 electrodes are displayed in Figure 7e, which are achieved by a chopped illumination of UV–visible light at an interval of 10 s on/off switch. The photoresponse performance of three α-Fe_2O_3/GO electrodes displays as fast, steady, and reproducible characteristic as that of pure α-Fe_2O_3 electrode. The photocurrent density of α-Fe_2O_3/GO 3 electrode is about 1.96 times higher than that of pure α-Fe_2O_3 electrode, which is consistent with the photocurrent-potential results in Figure 7c. The chopping photocurrent-potential plots in Figure 7f also display rapid photoresponse as that in const potential in Figure 7c. The α-Fe_2O_3/GO 3 electrode exhibits the highest photocurrent again, confirming it is an efficient and stable photoelectrode in any potential applied in this experiment.

In order to further discuss the important role of the graphene oxide in enhancing the photocurrent response performance of α-Fe_2O_3/graphene oxide composites, a schematic mechanism of UV–visible light-induced charge transfer and separation process has been proposed in **Figure 8**. The unique morphological and structural feature of α-Fe_2O_3 tetrakaidecahedron offers the favorable photocatalytic activity with abundant exposed single-crystal facts and massive active reacting sites of uncoordinated surface atoms.[14,50] In the diagram, mobile electrons are photoexcited into conducting band of α-Fe_2O_3 when incident photons with appropriate energy are absorbed by the hematite and holes are created in the valence band of α-Fe_2O_3.[61] The suitable allocation between the work function of graphene and conducting band of hematite facilitates the light-induced electrons to quickly transfer from hematite to graphene.[55] During the photoelectrochemical reaction, the electrons can mobile on the broad surface of graphene to arrive the charge collector, resulting in the decrease of resistance of charge transfer and enhancement of the photocurrent. The photogenerated holes also can transfer from α-Fe_2O_3 to graphene due to the faster speed of reacting with water and longer lifetime of holes in graphene sheets.[38] The remove of holes changes the reacting interface of holes and water from α-Fe_2O_3 to graphene, which will accelerate the reaction kinetic of oxygen evolution reaction and lower the onset potential.[55] The doping of graphene in the composites during this experiment improves the photocurrent performance of α-Fe_2O_3 polyhedron with a faster response than the other report.[31] In the composite, graphene not only serves as a conducting substrate to transport more photogenerated electrons to charge collector, promotes the charge separation, reduces the charge carrier recombination, but also speeds up the electrochemical reaction rate, finally leading to a distinct increase in the photocurrent response.

3. Conclusion

In summary, novel composites composing of α-Fe_2O_3 tetrakaidecahedron and graphene oxide have been facilely constructed for the first time. Tetrakaidecahedronal α-Fe_2O_3 nanostructures have been easily synthesized by a hydrothermal process without any organic additives. After that, the hematite production is coupled with graphene by a simple hydrothermal reaction. The α-Fe_2O_3 tetrakaidecahedrons have been indicated to anchor well on the surface of graphene, leading to the successfully interfacial contact of hematite particles and graphene oxide. The photoelectrodes made of α-Fe_2O_3/graphene oxide composite have been demonstrated to display efficient photoelectrochemical activity and good reproducibility. Graphene can extract the photogenerated electrons from α-Fe_2O_3, which enhance the charge transfer and separation and suppress the charge recombination of electron–hole pairs, leading to the enhancement of photocurrent response. This unique composite not only has promising application in the field of efficient PEC water oxidation but also provides an effective route to fabricate new semiconductor/graphene photocatalysts with high performance in heterogeneous catalysis, water pollution decomposition, and dye-sensitized solar cells.

4. Experimental Section

Fabrication of GO: The preparation of graphene oxide was followed by the previous publications[62,63] through a modified Hummers method. First, graphite flake (5 g, average diameter of 4 μm, purity of 99.95%, Qingdao Tianhe Graphite Co. Ltd., Qingdao, China) and $NaNO_3$ (3.75 g, purity of A.R.) were put into a flask. After that, concentrated H_2SO_4 (375 mL, purity of A.R.) was poured into the flask slowly while

stirring in the bath of ice-water. After 1 h, $KMnO_4$ (22.5 g, purity of A.R.) was added carefully and kept stirring for another 2 h. After stirring the mixture for 5 d at room temperature, another 700 mL H_2SO_4 aqueous solution was added (5 wt%, purity of A.R.) slowly for about 1 h. The temperature was raised to 98 °C and kept for 2 h under stirring. Afterward, the temperature was reduced to 60 °C and 15 mL H_2O_2 (30 wt% aqueous solution) was added. The mixture was then stirred for 2 h and kept at room temperature. The purifying procedure was repeated for 15 times to remove impurity in the resultant mixture, which included high-speed centrifugation, removal of the superfluous liquid, adding 2 L mixture of H_2SO_4 (3 wt%) and H_2O_2 (0.5 wt%), and dispersing the solid with vigorous stirring and bath ultrasonication (140 W) for 30 min. A similar process was repeated with different clearing liquid: HCL aqueous solution (2 L, 3 wt%) three times and H_2O (2 L) one time. The remaining HCL acid ions were removed by passing the eventual water solution through a weak basic ion-exchange resin (D301T, Nankai University Chemical Plant) with water as mobile phase. After removal of water by a drying process, the yield of product was about 3.5 g.

Fabrication of Fe_2O_3–Graphene Composites: In a typical experiment, 0.0795 g $FeCl_2{\cdot}4H_2O$ (Sinopharm Chemical Reagent Corp., ≥99%) was added into 60 mL H_2O to form solution A. Then, 4 g NaOH (Sinopharm Chemical Reagent Corp., ≥99%) was dissolved in 100 mL H_2O to obtain solution B. 5 mL of solution B was added to solution A in a slow rate of 4 mL h^{-1} by dropwise to induce a precipitation reaction under vigorous stirring. After that, the resultant mixture was transferred into a Teflon-lined autoclave, sealed tightly, and heated at 160 °C for 600 min. Following natural cooling to room temperature, the solid production was collected by centrifugation at 12 000 rpm for 7 min and washed with deionized water and ethanol for three times, respectively. The production was then dried in the oven at 60 °C for 360 min and further treated at 300 °C for 120 min in air to obtain the final α-Fe_2O_3 tetrakaidecahedron. The α-Fe_2O_3-graphene composites were fabricated through an ex situ route.[64,65] The mixture containing different amount of GO and α-Fe_2O_3 nanoparticles was added in a Teflon-lined autoclave and maintained at 160 °C for 12 h. Afterward, the autoclave was naturally cooled to ambient temperature. The α-Fe_2O_3/graphene oxide hybrids with different weight ratios of GO to α-Fe_2O_3 were fabricated by adjusting the addition amounts of GO. Subsequently, the composites were collected by centrifugation and dried at 60 °C in air for further characterization.

Structural Characterization: The obtained α-Fe_2O_3 nanoparticles and α-Fe_2O_3/graphene oxide composites with different weight ratios of GO were characterized by X-ray diffraction using Cu Kα radiation (XRD, Bruker D8-A25), field-emission scanning electron microscope (FESEM, JSM-6701F), transmission electron microscope (TEM, CM200FEG). The XPS spectra were measured by a Perkin Elmer PHI 5000 C ESCA system coupled with a hemispherical electron energy analyzer. The Mg-Kα (1253.6 eV) anode was operated at 14 kV and 20 mA. The Fourier transform infrared spectroscopy and Raman spectra were collected on Nexus 470 FT-IR spectrometer and Spex 403 Raman spectrometer.

Photoelectrochemical Measurements: Photoelectrochemical investigation was conducted with a standard three-electrode cell containing a working electrode, a Pt wire as the counter electrode, and a mercurous sulfate electrode as the reference electrode and performed by an electrochemical workstation (CHI 600e, CH Instruments) under a 50 W Xe lamp (HSX-F300, Beijing NBET Technology Co., Ltd). The potentials were converted to the RHE. A solution of 0.1 M Na_2SO_4 (Sinopharm Chemical Reagent Corp., ≥99%) was used as the supporting electrolyte after bubbling with high-purity N_2 for 30 min before the measurements. The working electrode was fabricated by an indium-tin oxide (ITO) glass deposited with production samples. During a process of making a working electrode, production sample (1 mg) was completely dispersed in a solution, which contained water (0.5 mL), alcohol (0.5 mL), and 5 wt% Nafion solution (10 µL). The solution was ultrasonicated for 2 h to make a homogeneous ink. 200 µL of ink with a pipettor was taken and spread onto an ITO glass by dropwise to make an electrode of catalyst. Subsequently, the electrode was dried in air and then was ready for further characterization.

Acknowledgements

The work was supported by the National Natural Science Foundation of China (Grant No. 51471051), Science and Technology Commission of Shanghai Municipality (Grant Nos. 15520720700 and 13NM1400300), Shanghai Shu Guang Project (12SG01), the Programs for Professor of Special Appointment (Eastern Scholar) at Shanghai Institutions of Higher Learning, and China Postdoctoral Science Foundation (Grant No. 2014M560294). Part of the experimental work was carried out in Fudan Nanofabrication Laboratory.

Received: December 24, 2015
Revised: January 25, 2016
Published online: March 15, 2016

[1] a) T. R. Cook, D. K. Dogutan, S. Y. Reece, Y. Surendranath, T. S. Teets, D. G. Nocera, *Chem. Rev.* **2010**, *110*, 6474; b) H. Dotan, O. Kfir, E. Sharlin, O. Blank, M. Gross, I. Dumchin, G. Ankonina, A. Rothschild, *Nat. Mater.* **2013**, *12*, 158.
[2] S. C. Han, Y. C. Pu, L. X. Zheng, J. Z. Zhang, X. S. Fang, *J. Mater. Chem. A* **2015**, *3*, 22627.
[3] J. Brillet, M. Gratzel, K. Sivula, *Nano Lett.* **2010**, *10*, 4155.
[4] L. Steier, I. H.-Cardona, S. Gimenez, F. F.-Santiago, J. Bisquert, S. D. Tilley, M. Gratzel, *Adv. Funct. Mater.* **2014**, *24*, 7681.
[5] D. A. Wheeler, G. M. Wang, Y. C. Ling, Y. Li, J. Z. Zhang, *Energy Environ. Sci.* **2012**, *5*, 6682.
[6] W. P. Yi, M. N. Chong, T. Zhu, S. T. Yong, E. S. Chan, *Mater. Res. Bull.* **2015**, *69*, 71.
[7] S. C. Han, L. F. Hu, Z. Q. Liang, S. Wageh, A. A. Al-Ghamdi, Y. S. Chen, X. S. Fang, *Adv. Funct. Mater.* **2014**, *24*, 5719.
[8] T. K. Townsend, E. M. Sabio, N. D. Browning, F. E. Osterloh, *Energy Environ. Sci.* **2011**, *4*, 4270.
[9] Y. Ling, G. Wang, D. A. Wheeler, J. Z. Zhang, Y. Li, *Nano Lett.* **2011**, *11*, 2119.
[10] N. K. Chaudhari, H. C. Kim, M. S. Kim, J. Park, J. S. Yu, *CrystEngComm* **2012**, *14*, 2024.
[11] A. Annamalai, A. G. Kannan, S. Y. Lee, D.-W. Kim, S. H. Choi, J. S. Jang, *J. Phys. Chem. C* **2015**, *119*, 19996.
[12] F. Meng, S. A. Morin, S. Jin, *J. Am. Chem. Soc.* **2011**, *133*, 8408.
[13] L. S. Zhong, J. S. Hu, H. P. Liang, A. M. Cao, W. G. Song, L. J. Wan, *Adv. Mater.* **2006**, *18*, 2426.
[14] W. Wu, R. Hao, F. Liu, X. Su, Y. Hou, *J. Mater. Chem. A* **2013**, *1*, 6888.
[15] W. W. Zhou, C. W. Cheng, J. P. Liu, Y. Y. Tay, J. Jiang, X. T. Jia, J. X. Zhang, H. Gong, H. H. Hng, T. Yu, H. J. Fan, *Adv. Funct. Mater.* **2011**, *21*, 2439.
[16] J. S. Chen, T. Zhu, X. H. Yang, H. G. Yang, X. W. Lou, *J. Am. Chem. Soc.* **2010**, *132*, 13162.
[17] Z. Y. Fan, X. G. Wen, S. H. Yang, J. G. Lu, *Appl. Phys. Lett.* **2005**, *87*, 013113.
[18] Z. Sun, H. Yuan, Z. Liu, B. Han, X. Zhang, *Adv. Mater.* **2005**, *17*, 2993.
[19] H. Katsuki, S. Komarneni, *J. Am. Ceram. Soc.* **2003**, *86*, 183.
[20] Y. Hou, F. Zuo, A. Dagg, P. Y. Feng, *Angew. Chem. Int. Ed.* **2013**, *58*, 1248.
[21] K. Y. Yoon, J. S. Lee, K. Kim, C. H. Bak, S. I. Kim, J. B. Kim, J. H. Jang, *ACS Appl. Mater. Interfaces* **2014**, *6*, 22634.
[22] B. Klahr, S. Gimenez, F. F. Santiago, J. Bisquert, T. W. Hamann, *Energy Environ. Sci.* **2012**, *5*, 7626.
[23] Y. Jun, J. Choi, J. Cheon, *Angew. Chem. Int. Ed.* **2006**, *45*, 3414.
[24] Z. Zhang, B. Xu, X. Wang, *Chem. Soc. Rev.* **2014**, *43*, 7870.
[25] J. Z. Yin, Z. N. Yu, F. Gao, J. J. Wang, H. Pang, Q. Y. Lu, *Angew. Chem. Int. Ed.* **2010**, *49*, 6328.

[26] B. L. Lv, Z. Y. Liu, H. Tian, Y. Xu, D. Wu, Y. H. Sun, *Adv. Funct. Mater.* **2010**, *20*, 3987.
[27] Y. Yang, H. X. Ma, J. Zhuang, X. Wang, *Inorg. Chem.* **2011**, *50*, 10143.
[28] T. K. Van, H. G. Cha, C. K. Nguyen, S.-W. Kim, M.-H. Jung, Y. S. Kang, *Cryst. Growth Des.* **2012**, *12*, 862.
[29] R. M. Liu, Y. W. Jiang, H. Fan, Q. Y. Lu, W. Du, F. Gao, *Chem. Eur. J.* **2012**, *18*, 8957.
[30] X. L. Li, W. J. Wei, S. Z. Wang, L. Kuai, B. Y. Geng, *Nanoscale* **2011**, *3*, 718.
[31] R. Xu, Y. Xu, Y. Huang, Y. M. Shi, B. Zhang, *CrystEngComm* **2015**, *17*, 27.
[32] J. Y. Kim, G. Magesh, D. H. Youn, J. W. Jang, J. Kubota, K. Domen, J. S. Lee, *Sci. Rep.* **2013**, *3*, 2681.
[33] B. Klahr, S. Gimenez, F. Fabregat-Santiago, J. Bisquert, T. W. Hamann, *J. Am. Chem. Soc.* **2012**, *134*, 16693.
[34] S. D. Tilley, M. Cornuz, K. Sivula, M. Gratzel, *Angew. Chem. Int. Ed.* **2010**, *49*, 6405.
[35] H. Chang, H. K. Wu, *Adv. Funct. Mater.* **2013**, *23*, 1984.
[36] N. Gao, X. S. Fang, *Chem. Rev.* **2015**, *115*, 8294.
[37] Y. Hou, F. Zuo, A. Dagg, P. Y. Feng, *Nano Lett.* **2012**, *12*, 6464.
[38] H. M. Zhang, C. L. Zhu, Y. J. Chen, M. Yang, P. P. Yang, X. H. Wu, L. H. Qi, F. N. Meng, *J. Mater. Chem. A* **2015**, *3*, 1421.
[39] Y. B. Zhao, F. Pan, H. Li, T. C. Niu, G. Q. Xu, W. Chen, *J. Mater. Chem. A* **2013**, *1*, 7242.
[40] J. S. Chen, X. Chen, Y. M. Li, X. L. Chen, R. V. Ramanujan, X. Hu, *RSC Adv.* **2014**, *4*, 593.
[41] C. Xu, X. Wang, J. Zhu, X. Yang, L. Lu, *J. Mater. Chem.* **2008**, *18*, 5625.
[42] L. Q. Jing, Y. Cao, H. Q. Cui, J. R. Durrant, J. W. Tang, D. N. Liu, H. G. Fu, *Chem. Commun.* **2012**, *48*, 10775.
[43] J. Liu, H. Bai, Y. Wang, Z. Liu, X. Zhang, D. D. Sun, *Adv. Funct. Mater.* **2010**, *20*, 4175.
[44] G. Titelman, V. Gelman, S. Bron, R. Khalfin, Y. Cohen, H. Bianco-Peled, *Carbon* **2005**, *43*, 641.
[45] M. Li, S. K. Cushing, X. Zhou, S. Guo, N. Q. Wu, *J. Mater. Chem.* **2012**, *22*, 23374.
[46] L. W. Zhang, H. B. Fu, Y. F. Zhu, *Adv. Funct. Mater.* **2008**, *18*, 2180.
[47] J. F. Zang, S. J. Bao, C. M. Li, H. J. Bian, X. Q. Cui, Q. L. Bao, C. Q. Sun, J. Guo, K. R. Lian, *J. Phys. Chem. C* **2008**, *112*, 14843.
[48] A. D. Fabio, A. Giorgi, M. Mastragostino, F. Soavi, *J. Electrochem. Soc.* **2001**, *148*, A845.
[49] N. J. Bell, Y. H. Ng, A. Du, H. Coster, S. C. Smith, R. Amal, *J. Phys. Chem. C* **2011**, *115*, 6004.
[50] X. Zhou, J. Lan, G. Liu, K. Deng, Y. Yang, G. Nie, J. Yu, L. Zhi, *Angew. Chem. Int. Ed.* **2012**, *51*, 178.
[51] F. K. Meng, J. T. Li, S. K. Cushing, J. Bright, M. J. Zhi, J. D. Rowley, Z. L. Hong, A. Manivannan, A. D. Bristow, N. Q. Wu, *ACS Catal.* **2013**, *3*, 746.
[52] K. Sivula, R. Zboril, F. L. Formal, R. Robert, A. Weidenkaff, J. Tucek, J. Frydrych, M. Gratzel, *J. Am. Chem. Soc.* **2010**, *132*, 7436.
[53] K. Zhang, X. J. Shi, J. K. Kim, J. S. Lee, J. H. Park, *Nanoscale* **2013**, *5*, 1939.
[54] L. M. He, L. Q. Jing, Y. B. Luan, L. Wang, H. G. Fu, *ACS Catal.* **2014**, *4*, 990.
[55] A. G. Tamirat, W. N. Su, A. A. Dubale, C. J. Pan, H. M. Chen, D. W. Ayele, J. F. Lee, B. J. Hwang, *J. Power Sources* **2015**, *287*, 119.
[56] Y. H. Ng, A. Iwase, A. Kudo, R. Amal, *J. Phys. Chem. Lett.* **2010**, *1*, 2607.
[57] L. Jia, D. H. Wang, Y. X. Huang, A. W. Xu, H. Q. Yu, *J. Phys. Chem. C* **2011**, *115*, 11466.
[58] A. C. Nielander, M. J. Bierman, N. Petrone, N. C. Strandwitz, S. Ardo, F. Yang, J. Hone, N. S. Lewis, *J. Am. Chem. Soc.* **2013**, *135*, 17246.
[59] Y. Bai, J. Wu, J. Xi, J. Wang, W. Zhu, L. Chen, X. Qiu, *Electrochem. Commun.* **2005**, *7*, 1087.
[60] Q. P. Wu, J. Zhao, K. Liu, H. Y. Wang, Z. Sun, P. Li, S. Xue, *Int. J. Hydrogen Energy* **2015**, *40*, 6763.
[61] R. C. Pawar, D.-H. Choi, C. S. Lee, *Int. J. Hydrogen Energy* **2015**, *40*, 767.
[62] H. A. Becerril, J. Mao, Z. F. Liu, R. M. Stoltenberg, Z. N. Bao, Y. S. Chen, *ACS Nano* **2008**, *2*, 463.
[63] M. Hirata, T. Gotou, S. Horiuchi, M. Fujiwara, M. Ohba, *Carbon* **2004**, *42*, 2929.
[64] Z. Y. Wang, C. J. Liu, *Nano Energy* **2015**, *11*, 277.
[65] H. Zhang, A. J. Xie, C. P. Wang, H. S. Wang, Y. H. Shen, X. Y. Tian, *J. Mater. Chem. A* **2013**, *1*, 8547.